ChemComm

ROYAL SOCIETY OF CHEMISTRY

COMMUNICATION

View Article Online
View Journal | View Issue

Cite this: *Chem. Commun.*, 2025, **61**, 1463

Received 30th September 2024,
Accepted 17th December 2024

DOI: 10.1039/d4cc05105j

rsc.li/chemcomm

From single atoms to nanoparticles: size effect on Pd/C-catalyzed hydrogenation of 2,5-furandicarboxylic acid†

Jiali Zheng,[a] Zhihui Li,*[ab] Dongsheng Zhang,[a] Xinqiang Zhao,[a] Qian Zhao[a] and Yanji Wang*[a]

In this study, five catalysts with Pd particle sizes ranging from single atoms to nanoclusters and nanoparticles were synthesized by controlling the Pd loading amount and preparation methods, and applied in the hydrogenation of FDCA to THFDCA. Furthermore, kinetic models were established. Notably, the nanocluster catalyst demonstrated relatively high hydrogenation activity.

One of the important types of heterogeneous catalysts is supported metal catalysts, which are extensively utilized in fine chemical synthesis and various industrial chemical reactions.[1–3] Moreover, the "size effect" is a crucial factor affecting the activity and selectivity of supported metal catalysts.[4–7] As the size of metal particles decreases to the nanoscale, their electronic and geometric structures change significantly, endowing them with several excellent properties.[8–11] Li *et al.*[12] prepared Pd nanoparticles of varying sizes *via* a stepwise growth reaction and examined their catalytic performance in the Suzuki reaction between phenylboric acid and iodobenzene. The results revealed that the catalytic activity of Pd nanoparticles decreased with increasing particle size. According to Haruta *et al.*,[13] Au nanoparticles smaller than 5 nm exhibit high CO oxidation activity at −73 °C, overturning the perception that Au is an inert metal in catalysis. The changes in the size of metal nanoparticles influence the geometric and electronic structure of the supported metal catalyst, thereby regulating its catalytic performance, as demonstrated by the Fischer–Tropsch reaction catalyzed by Co,[14,15] the methane dry reforming reaction catalyzed by Ni,[16,17] and the synthetic ammonia reaction catalyzed by Ru.[18] Therefore, the design of highly active and selective nanoparticles, nanoclusters, and even single-atom supported metal catalysts through the precise regulation of the size of metal nanoparticles has garnered widespread attention from researchers.[19–22]

Adipic acid (AA) is a dicarboxylic acid characterized by considerable industrial significance and practical value and is an essential monomer in the production of nylon 66 and polyurethane. Currently, the global annual production of AA exceeds 3 million tons, with demand increasing at a rate of 3–5% per year.[23] The conventional production of AA relies on the inefficient oxidation process of petroleum-derived cyclohexane, using highly corrosive concentrated nitric acid as the oxidant. However, this process presents issues like low one-way yield, equipment corrosion, and powerful greenhouse gas NO_x. Considering the internal requirements of a dual-carbon strategy and sustainable development, it is imperative to develop a green and renewable AA production process.

Notably, 5-hydroxymethylfurfural (HMF) is characterized by its active aldehyde and hydroxyl groups and can be transformed into chemical intermediates like 5-hydroxymethylfurfuryl alcohol, 2, 5-diformylfuran, and 2,5-furandicarboxylic acid (FDCA) through hydrogenation, oxidation, and ring-opening reactions. It serves as a conduit between biomass resources and high-value chemicals.[24,25] Recently, the production of bio-based AA from HMF *via* FDCA synthesis and conversion has become a promising approach. Our research group has successfully developed a four-step reaction pathway for the synthesis of bio-based AA from HMF (Scheme 1). These steps include the anaerobic dehydrogenation of HMF to prepare DFF,[26] the one-step synthesis of FDCA from DFF and hydroxylamine under anaerobic conditions,[27] the preparation of 2,5-tetrahydrofurandicarboxylic acid (THFDCA) through the double bond hydrogenation of FDCA, and the synthesis of AA through the hydrogenation deoxygenation of THFDCA. This paper mainly focuses on step III: FDCA double bond hydrogenation to THFDCA,

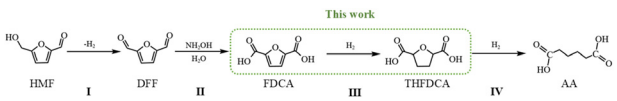

Scheme 1 HMF synthesis AA flowchart.

[a] School of Chemical Engineering and Technology, Hebei University of Technology, Tianjin 300401, China. E-mail: yjwang@hebut.edu.cn
[b] School of Energy and Environmental Engineering, Hebei University of Technology, Tianjin 300401, China. E-mail: lizhihui425@hebut.edu.cn

† Electronic supplementary information (ESI) available. See DOI: https://doi.org/10.1039/d4cc05105j

from the whole new process route of HMF synthesis of AA, FDCA double-bond hydrogenation to THFDCA is an essential step. Therefore, this work has important theoretical and practical value. At present, there are few reports about the preparation of THFDCA by FDCA, and there is no report on the study of the size effect of the reaction.

In 2016, Asano *et al.*[28] reported the hydrogenation of FDCA catalyzed by Pt–MoO_x/TiO_2 in aqueous solvent, thereby achieving a 20% THFDCA yield under conditions of 1.5 MPa H_2 at 140 °C for 4 h. Wei *et al.*[29] examined the hydrogenation of FDCA catalyzed by Pt/CeO_2 using water as the solvent. Here, the conversion of FDCA was 71%, and the selectivity of THFDCA was 58% at 3 MPa H_2 and 200 °C for 4 h. Furthermore, Rennova Company[30] analyzed the FDCA hydrogenation reaction catalyzed by Pd/SiO_2, achieving a THFDCA yield of 88% under conditions of 5.2 MPa H_2 and 140 °C for 3 h.

The Pd-based catalysts demonstrate strong adsorption and activation capabilities for hydrogen and unsaturated substrates due to their unique electronic structure, resulting in extremely high FDCA hydrogenation activity.[31] Activated carbon, as a carrier, has the advantages of low price, stable chemical properties, acid and alkali resistance, high-temperature resistance, developed pore structure, and excellent adsorption performance. Based on this, this paper presents the design and synthesis of activated carbon-supported Pd catalysts (Pd/C) with varying sizes ranging from a single atom to nanoclusters (1–2 nm) and then to nanoparticles (>2 nm) by adjusting the Pd loading amount and preparation method. Additionally, the size effect on the catalytic hydrogenation of FDCA to THFDCA is analyzed. As per the results, the nanocluster Pd/C catalyst demonstrated the highest hydrogenation activity.

The actual Pd content of Pd/C samples was measured using ICP-AES/MS (Table 1). The morphology and particle size of the Pd/C catalysts with different loading amounts were determined through transmission electron microscopy (TEM) and aberration-corrected HAADF-STEM characterization (see Fig. 1). The maximum average particle size of Pd particles was 3.78 nm when the Pd loading was 3.63%, and the Pd nanoparticles were uniformly dispersed on the surface of the carrier (Fig. 1A). Moreover, the average particle size of Pd particles gradually decreases as the Pd loading reduces. As the loading reduces to 1.98%, 0.99%, and 0.20%, the average particle size of Pd particles decreases to 2.10, 1.83, and 1.09 nm, respectively, and is highly dispersed (Fig. 1B–D). The presence of Pd single atoms becomes evident as the Pd loading is further reduced to 0.09% (Fig. 1E). Notably, the particle size of Pd nanoparticles can be

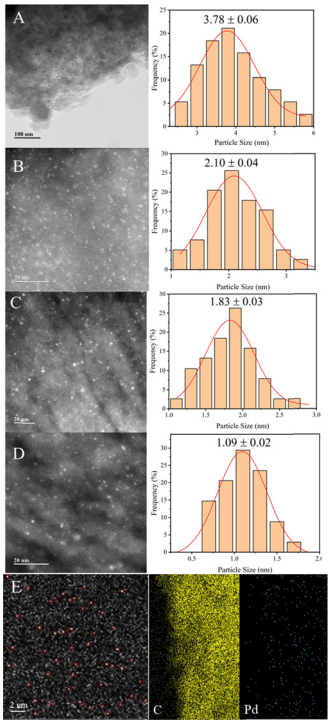

Fig. 1 HAADF-STEM images of Pd/C catalysts with different Pd loadings: (A) 3.63%; (B) 1.98%; (C) 0.99%; (D) 0.20%; (E) aberration-corrected HAADF-STEM images of 0.09%Pd/C.

effectively regulated by adjusting the Pd loading amount, facilitating the synthesis of Pd/C catalysts with sizes ranging from nanoparticles to nanoclusters and then to single atoms.

The dispersion of Pd was detected *via* the CO chemisorption test. As displayed in Table 1, the variation trend of the dispersion of Pd particles is opposite to that of particle size. The dispersion of Pd gradually increases as the Pd loading decreases. At a Pd loading of 0.20%, the maximum dispersion of Pd particles was 95.35%. The single-atom Pd was obtained by further reducing the Pd load to 0.09%. The Pd particle size calculated by this method aligns with the results obtained *via* the TEM method.

Fig. S1 (ESI†) illustrates the XRD patterns of five Pd/C catalysts with different particle sizes. Notably, two characteristic diffraction peaks are observed at 22.8° and 42.6°, which are attributed to activated carbon. Nevertheless, no relevant diffraction peaks of Pd (generally located near 40.1°, 46.6°, and 68°) are observed in the XRD pattern. This suggests that the Pd nanoparticles in the catalyst are

Table 1 hysical properties of Pd/C catalysts

		CO chemisorption[c]		
Samples[a] (nm)	Pd loading[b] (%)	CO uptake ($\mu mol_{CO}\ g^{-1}$)	Pd dispersion (%)	Pd particle size (nm)
3.78	3.63	55.85	29.70	3.77
2.10	1.98	48.59	51.70	2.16
1.83	0.99	27.14	57.76	1.94
1.09	0.20	4.48	95.35	1.18
SA	0.09	9.62	100	—

[a] Measured by HAADF-STEM and TEM images. [b] Measured by ICP-AES/MS. [c] Calculated based on CO titration.

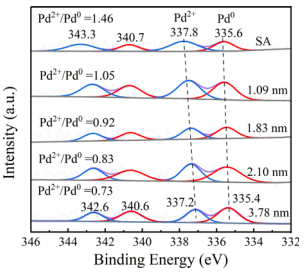

Fig. 2 XPS spectra of the Pd/C catalysts in the Pd 3d region.

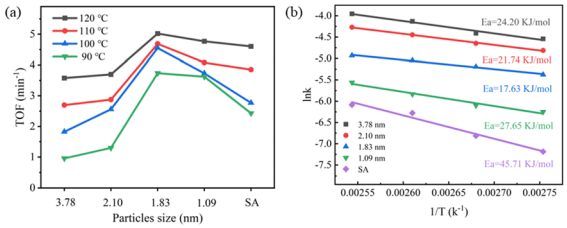

Fig. 3 (a) Comparison of FDCA hydrogenation activity on Pd/C catalysts with different sizes (b) Arrhenius curves of FDCA hydrogenation to THFDCA on Pd/C catalysts of different sizes.

extremely small and uniformly dispersed on the surface of the activated carbon carrier.[32]

Subsequently, the electronic properties of Pd species in Pd/C catalysts were analyzed through XPS. Here, two sets of double peaks were observed in the Pd 3d region, attributed to Pd $3d_{5/2}$ and Pd $3d_{3/2}$, respectively. Among them, the peaks at 335.6 and 340.7 eV of binding energy corresponding to Pd^0, while the peaks at 337.8 and 343.3 eV are related to Pd^{2+}, and the ratio of Pd^{2+}/Pd^0 gradually decreases with the increase of Pd size, which is consistent with the conclusions reported in the literature.[32–35] In addition, it can be seen from Fig. 2 that with the decrease of the palladium particle size, the peaks of Pd^0 and Pd^{2+} are shifted to the direction of high binding energy, indicating that the electron transfer process between the Pd species and the carrier has changed, and the smaller the particle size, the more electrons of Pd species flow to the carrier, and the more obvious the electron deficiency state of the Pd species.[10,36,37]

The effects of reaction time, hydrogen pressure, reaction temperature, and catalyst dosage on the performance of FDCA hydrogenation synthesis of THFDCA were investigated using $Pd_{3.78}$/C as the catalyst. Table S1 (ESI†) presents the results. The optimum conditions for the hydrogenation reaction with a $Pd_{3.78}$/C catalyst were obtained as follows: 0.1 g catalyst, 3 MPa H_2, 120 °C for 5 h, achieving 100% FDCA conversion, and 100% THFDCA yield. Next, the hydrogenation performance of four other catalysts with varying sizes was investigated under this condition. The results revealed that both FDCA conversion and THFDCA yield could reach 100% when $Pd_{2.10}$/C and $Pd_{1.83}$/C were used as catalysts. Upon using $Pd_{1.09}$/C and single-atom Pd/C as catalysts, the conversion of FDCA was 92.8% and 86.7%, respectively, while the yield of THFDCA reduced significantly to 11.6% and 3.8%. This can be attributed to the low content of active components in these two catalysts, resulting in insufficient surface active sites. It can also be attributed to the different sizes of the catalyst used.

To further explore the aforementioned reasons, the specific hydrogenation activity of catalysts with different loading amounts was compared through TOF (turnover frequency) values. First, to regulate the conversion of FDCA to be roughly the same, the catalyst amount and reaction time were reduced to 0.04 g and 60 min, respectively. Furthermore, changes in conversion over time with different catalyst loadings at varying temperatures were obtained through online sampling. Fig. S2 (ESI†) shows that the FDCA conversion is positively correlated with the Pd loading when the reaction temperature is constant. Thus, a larger Pd loading results in a higher FDCA conversion. Notably, the FDCA conversion is the highest across the entire temperature range when $Pd_{3.78}$/C is utilized as the catalyst, which is consistent with the maximum number of surface active sites. Moreover, the conversion of FDCA showed an overall upward trend with increasing temperature. The variation trend of THFDCA yield was consistent with the conversion.

As displayed in Fig. 3(a), TOF was calculated based on FDCA conversion data and was correlated with Pd/C catalyst particle size. It is noted that the TOF data exhibits a "volcanic" trend with Pd particle size, indicating that with decreasing Pd particle size, the hydrogenation-specific activity of the Pd/C catalyst initially increases and then decreases. Nanocluster catalysts demonstrate higher FDCA hydrogenation activity, with the Pd/C catalyst having a particle size of 1.83 nm showing the highest activity, achieving a TOF of 5.02 min^{-1} at 120 °C.

Fig. S2 and S3 (ESI†) depict the hydrogenation activity data of Pd/C catalysts of varying sizes in the range of 90–120 °C. In light of this, a reaction kinetics equation was constructed for the hydrogenation synthesis of THFDCA from FDCA. First, to verify whether the internal and external diffusion effects of the reaction system can be ignored, the Weisz–Prater criterion (C_{WP}) and Mears criterion (C_M)[38] were utilized. The calculation method can be seen in the ESI.† The calculation results displayed in Table S2 (ESI†) indicate that C_{wp} is below 1 and C_M is below 0.15. Hence, the influence of both internal and external diffusion can be ignored.

The kinetics of FDCA hydrogenation catalyzed by Pd/C with different sizes were calculated based on the conversion of FDCA at different times and temperatures. Ignoring the influence of internal and external diffusion, the rate equation of the hydrogenation reaction can be seen in the ESI.†

Fig. 3(b) displays the Arrhenius comparison of Pd/C catalysts with varying sizes. The figure shows that the apparent activation energy E_a, which is calculated according to the Arrhenius equation, gradually decreases with increasing Pd particle size. The activation energy decreases from the maximum of 45.71 kJ mol^{-1} at Pd_{SA}/C to 27.65 kJ mol^{-1} at 1.09 nm, and then to the minimum of 17.63 kJ mol^{-1} at 1.83 nm. It gradually increased to 21.74 kJ mol^{-1} at 2.10 nm and 24.20 kJ mol^{-1} at 3.78 nm. This is primarily due to the weaker H_2 dissociation ability of isolated Pd single atoms, whereas Pd nanoclusters are more favorable for H_2 dissociation.[38,39] Consequently, FDCA hydrogenation catalyzed by Pd_{SA}/C has the highest apparent activation energy, while the lowest apparent activation energy is

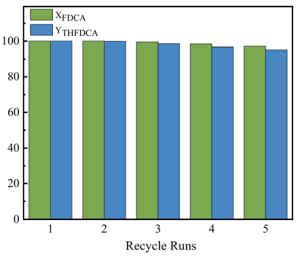

Fig. 4 Recycling of Pd/C.

associated with FDCA hydrogenation catalyzed by the $Pd_{1.83}$/C nanocluster catalyst, which is most conducive to FDCA conversion.

To evaluate the recovery and recycling performance of the Pd/C catalyst, the FDCA hydrogenation reaction was investigated using $Pd_{1.83}$/C as the catalyst under the aforementioned optimized conditions. After the reaction, the reaction liquid was cooled to room temperature. The catalyst was then centrifuged, washed three times with deionized water, vacuum dried at 100 °C for 12 h, and subsequently utilized for the next round of reaction. As noted in Fig. 4, after recycling the catalyst five times, the conversion of FDCA and the yield of THFDCA remain as high as 97.1% and 95.2%, respectively, implying that Pd/C has high stability and can be recycled multiple times while maintaining its structure and activity.

In conclusion, this study presents the synthesis of Pd/C catalysts ranging from single atoms to nanoparticles by controlling the Pd loading amount and preparation method. The results demonstrate the high activity of the Pd/C catalyst for the hydrogenation of FDCA to THFDCA. For the first time, the size effect of FDCA double-bond hydrogenation to THFDCA was systematically studied, and it was found that the particle size of Pd had a great influence on the hydrogenation activity of FDCA, and five Pd species of different sizes exhibit considerably different catalytic activities in the FDCA hydrogenation reaction. From single atom Pd to nanoparticle Pd, the catalytic activity demonstrates a "volcanic" trend with the particle size, demonstrating relatively high hydrogenation activity on the nanocluster catalyst. This activity attains its optimal level on the $Pd_{1.83}$/C, indicating that Pd nanoclusters have the optimal catalyst size for FDCA hydrogenation to THFDCA. This work clarified the specific effect of particle size on the synthesis of THFDCA, provided a theoretical basis for the construction of efficient FDCA hydrogenation catalyst, and provided a reference for the tetrahydride reaction of other furan compounds.

This work is supported by the National Natural Science Foundation of China (U20A20152, 21236001).

Data availability

The data supporting this article have been included as part of the ESI.†

Conflicts of interest

There are no conflicts to declare.

Notes and references

1 G. C. Bond, *Chem. Soc. Rev.*, 1991, **20**, 441–475.
2 L. Zhang, M. Zhou, A. Wang and T. Zhang, *Chem. Rev.*, 2020, **120**, 683–733.
3 L. Cao, W. Liu, Q. Luo, R. Yin, B. Wang, J. Weissenrieder, M. Soldemo, H. Yan, Y. Lin, Z. Sun, C. Ma, W. Zhang, S. Chen, H. Wang, Q. Guan, T. Yao, S. Wei, J. Yang and J. Lu, *Nature*, 2019, **565**, 631–635.
4 G. C. Bond, *Surf. Sci.*, 1985, **156**, 966–981.
5 M. Che and C. O. Bennett, *Adv. Catal.*, 1989, **36**, 55–172.
6 H. Wang and J. Lu, *Chin. J. Chem.*, 2020, **38**, 1422–1444.
7 J. K. Nørskov, T. Bligaard, B. Hvolbæk, F. Abild-Pedersen, I. Chorkendorff and C. H. Christensen, *Chem. Soc. Rev.*, 2008, **37**, 2163–2171.
8 N. Vilar-Vidal, J. Rivas and M. A. López-Quintela, *ACS Catal.*, 2012, **2**, 1693–1697.
9 S. Chen, L. Luo, Z. Jiang and W. Huang, *ACS Catal.*, 2015, **5**, 1653–1662.
10 J. Li, W. Chen, H. Zhao, X. Zheng, L. Wu, H. Pan, J. Zhu, Y. Chen and J. Lu, *J. Catal.*, 2017, **352**, 371–381.
11 X. Zhang, Q. Gu, Y. Ma, Q. Guan, R. Jin, H. Wang, B. Yang and J. Lu, *J. Catal.*, 2021, **400**, 173–183.
12 Y. Li, E. Boone and M. A. El-Sayed, *Langmuir*, 2002, **18**, 4921–4925.
13 M. Haruta, T. Kobayashi, H. Sano and N. Yamada, *Chem. Lett.*, 1987, 405–408.
14 R. van den Berg, G. Prieto, G. Korpershoek, L. I. van der Wal, A. J. van Bunningen, S. Lægsgaard-Jørgensen, P. E. de Jongh and K. P. de Jong, *Nat. Commun.*, 2016, **7**, 13057.
15 P. van Helden, I. M. Ciobîcă and R. L. J. Coetzer, *Catal. Today*, 2016, **261**, 48–59.
16 Y. Wang, H. Wang, A. H. Dam, L. Xiao, Y. Qi, J. Niu, J. Yang, Y. Zhu, A. Holmen and D. Chen, *Catal. Today*, 2020, **355**, 139–147.
17 G. Jones, J. G. Jakobsen, S. S. Shim, J. Kleis, M. P. Andersson, J. Rossmeisl, F. Abild-Pedersen, T. Bligaard, S. Helveg, B. Hinnemann, J. R. Rostrup-Nielsen, I. Chorkendorff, J. Sehested and J. K. Nørskov, *J. Catal.*, 2008, **259**, 147–160.
18 Á. Logadóttir and J. K. Nørskov, *J. Catal.*, 2003, **220**, 273–279.
19 C. Mochizuki, Y. Inomata, S. Yasumura, M. Lin, A. Taketoshi, T. Honma, N. Sakaguchi, M. Haruta, K. Shimizu, T. Ishida and T. Murayama, *ACS Catal.*, 2022, **12**, 6149–6158.
20 X. Deng, D. Alfonso, T.-D. Nguyen-Phan and D. R. Kauffman, *ACS Catal.*, 2022, **12**, 5921–5929.
21 N. Wang, X. Zhao, R. Zhang, S. Yu, Z. H. Levell, C. Wang, S. Ma, P. Zou, L. Han, J. Qin, L. Ma, Y. Liu and H. L. Xin, *ACS Catal.*, 2022, **12**, 4156–4164.
22 G. Zhang, F. Tang, X. Wang, L. Wang and Y.-N. Liu, *ACS Catal.*, 2022, **12**, 5786–5794.
23 M. Lang and H. Li, *ChemSusChem*, 2022, **15**, e202101531.
24 L. Hu, Z. Wu, Y. Jiang, X. Wang, A. He, J. Song, J. Xu, S. Zhou, Y. Zhao and J. Xu, *Renew. Sustainable Energy Rev.*, 2020, **134**, 110317.
25 H. Wang, C. Zhu, D. Li, Q. Liu, J. Tan, C. Wang, C. Cai and L. Ma, *Renew. Sustainable Energy Rev.*, 2019, **103**, 227–247.
26 X. Gao, Z. Li, S. Zhang, D. Zhang, X. Zhao, B. Zhang and Y. Wang, *Chem. Eng. J.*, 2024, **496**, 153775.
27 J. Zheng, Z. Li, D. Zhang, X. Zhao, Q. Zhao and Y. Wang, *Appl. Catal., A*, 2024, **685**, 119886.
28 T. Asano, M. Tamura, Y. Nakagawa and K. Tomishige, *ACS Sustainable Chem. Eng.*, 2016, **4**, 6253–6257.
29 L. Wei, J. Zhang, W. Deng, S. Xie, Q. Zhang and Y. Wang, *Chem. Commun.*, 2019, **55**, 8013–8016.
30 T. Boussie, *US Pat.*, 8501989B2, 2013.
31 K. Liu, R. Qin and N. Zheng, *J. Am. Chem. Soc.*, 2021, **143**, 4483–4499.
32 Y. Kim and D. H. Kim, *Appl. Catal., B*, 2019, **244**, 684–693.
33 X. Gao, C. A. J. Fisher, T. Kimura, Y. H. Ikuhara, A. Kuwabara, H. Moriwake, H. Oki, T. Tojigamori, K. Kohama and Y. Ikuhara, *J. Mater. Chem. A*, 2014, **2**, 843–852.
34 Y. Xiao, L. Liang, Z. Liu, X. Yin, X. Yang, Y. Ding and Z. Du, *Appl. Surf. Sci.*, 2022, **585**, 152668.
35 S. Zhang, B. Jiang, K. Jiang and W.-B. Cai, *ACS Appl. Mater. Interfaces*, 2017, **9**, 24678–24687.
36 X. Zhou, Y. Huang, W. Xing, C. Liu, J. Liao and T. Lu, *Chem. Commun.*, 2008, 3540–3542.
37 W. P. Zhou, A. Lewera, R. Larsen, R. I. Masel, P. S. Bagus and A. Wieckowski, *J. Phys. Chem. B*, 2006, **110**, 13393–13398.
38 S. T. Oyama, X. Zhang, J. Lu, Y. Gu and T. Fujitani, *J. Catal.*, 2008, **257**, 1–4.
39 L. Kuai, Z. Chen, S. Liu, E. Kan, N. Yu, Y. Ren, C. Fang, X. Li, Y. Li and B. Geng, *Nat. Commun.*, 2020, **11**, 48.

